2000

# Entry of Plasma Sheet Particles into the Inner Magnetosphere Observed by POLAR/CAMMICE

N Yu Ganushkina

T I. Pulkkinen

V A. Sergeev

M V. Kubyshkina

D N. Baker

*See next page for additional authors*

JOURNAL OF GEOPHYSICAL RESEARCH, VOL. 105, NO. A11, PAGES 25,205–25,219, NOVEMBER 1, 2000

# Entry of plasma sheet particles into the inner magnetosphere as observed by Polar/CAMMICE

N. Yu. Ganushkina,[1,2] T. I. Pulkkinen,[1] V. A. Sergeev,[3] M. V. Kubyshkina,[3] D. N. Baker,[4] N. E. Turner,[4] M. Grande,[5] B. Kellett,[5] J. Fennell,[6] J. Roeder,[6] J.-A. Sauvaud,[7] and T. A. Fritz[8]

**Abstract.** Statistical results are presented from Polar/CAMMICE measurements of events during which the plasma sheet ions have penetrated deeply into the inner magnetosphere. Owing to their characteristic structure in energy-time spectrograms, these events are called "intense nose events." Almost 400 observations of such structures were made during 1997. Intense nose events are shown to be more frequent in the dusk than in the dawn sector. They typically penetrate well inside $L = 4$, the deepest penetration having occurred around midnight and noon. The intense nose events are associated with magnetic (substorm) activity. However, even moderate activity ($AE =$ 150–250 nT) resulted in formation of these structures. In a case study of November 3, 1997, three sequential inner magnetosphere crossings of the Polar and Interball Auroral spacecraft are shown, each of which exhibited signatures of intense nose-like structures. Using the innermost boundary determinations from these observations, it is demonstrated that a large-scale convective electric field alone cannot account for the inward motion of the structure. It is suggested that the intense nose structures are caused by short-lived intense electric fields (in excess of ~1 mV/m) in the inner tail at $L$=4–5.

## 1. Introduction

The ring current encircling the Earth in the range $L$=3–5 is carried mainly by energetic ions roughly in the energy interval 30 to 300 keV [*Daglis et al.*, 1999]. Further away, the plasma sheet has a characteristic ion temperature of a few keV. During magnetically quiet periods, these populations are quite distinct and are also separated in space. On the other hand, during disturbed periods, plasma sheet particles can penetrate to the inner magnetosphere even inside the plasmapause.

*Smith and Hoffman* [1974] found storm time ion enhancements inside the plasmapause with characteristic "nose" structures in the 90° pitch angle ion spectrograms from Explorer 45. The Explorer 45 data covered the equatorial inner magnetosphere ($L < 5$) in the afternoon to midnight sector. *Ejiri et al.* [1980] examined the nose structures observed by Explorer 45 in more detail and described the pertinent features of these events. They showed that the nose structures appear at low $L$ values all the way to the plasmapause with flux increases in the energy range of 15–25 keV. At larger $L$ values, both the higher-energy and lower-energy particle fluxes show further increase. The highest probability of occurence was found to be at 2000 magnetic local time (MLT).

Many other studies have been devoted to the ion distributions at $4 < L < 7$ based on observations from both equatorial spacecraft [*McIlwain*, 1972; *Kistler et al.*, 1989; *Sergeev et al.*, 1991, 1998] and from polar-orbiting satellites [*Shirai et al.*, 1997; *Fennell et al.*, 1998; *Peterson et al.*, 1998]. Most studies assumed that plasma sheet particles in the ring current region entered from the plasma sheet as a consequence of effects caused by convection, corotation, and magnetic gradient and curvature drifts. Thus the nose structures play an important role in the plasma sheet-ring current interaction.

Substorms are known to change the plasma configuration in the inner magnetosphere: during the growth

[1]Geophysical Research, Finnish Meteorological Institute, Helsinki, Finland.
[2]On leave from Skobeltsyn Institute of Nuclear Physics Moscow State University, Moscow, Russia.
[3]Institute of Physics, University of St.-Petersburg, St.-Petersburg, Russia.
[4]Laboratory for Atmospheric and Space Physics, University of Colorado, Boulder.
[5]Rutherford Appleton Laboratory, Chilton, Didcot, United Kingdom.
[6]The Aerospace Corporation, Los Angeles, California.
[7]Centre d'Etude Spatial des Rayonnements, Toulouse, France.
[8]Boston University, Boston, Massachusetts.



Paper number 2000JA900062.
0148-0227/00/2000JA900062$09.00

phase, the plasma sheet moves earthward, and at substorm onset energetic particles are injected at or near geosynchronous orbit (see *Baker et al.* [1996] and references therein). *Friedel et al.* [1996] examined data from the CRRES satellite in a near-equatorial orbit to find the locations of nearly dispersionless injections associated with substorm onsets. They showed that the injections can occur deep in the inner magnetosphere to $L = 4.3$ and that they are distributed up to ±5 hours in local time around local magnetic midnight. Thus these dispersionless injections occur in the same location where the nose structures are observed.

*Ejiri* [1978], *Ejiri et al.* [1980], and *Ebihara et al.* [1998] tried to interpret the observed patterns in terms of the temporal history of energetic ion distributions formed at the beginning of the storm main phase by a sudden enhancement of the electric field. *Sergeev et al.* [1991] studied a long period of steady magnetospheric convection and analyzed the ion motion using single-particle drifts from the tail in realistic magnetic and electric fields (Volland-Stern model in Ejiri 's calculations). They found that in that case the time stationary fields were adequate to reproduce the observed plasma distributions including both protons and electrons in the range of auroral energies (1–20 keV) as well as to accurately give the plasmapause (cold plasma) position. *Ebihara et al.* [1998] studied the enhancements of a directional differential flux of energetic particles in the inner magnetosphere taking into account the induced dawn-dusk electric field due to dipolarization during the substorm onset. The calculations showed good agreement with Explorer 45 observations. Thus at least for some events, the adiabatic drift theory explains reasonably well both penetration distances and MLT dependence of nose structures, but many open questions remain. For example, previous studies have not demonstrated whether typical convection electric fields can account for the inward injection or the formation of reverse gradients in the radial pressure distribution.

When examining particle entry, it is critically important to know the electric field distribution in the inner magnetosphere. Typical values of this electric field range from fractions of a millivolt per meter to ~1 mV/m [*Mozer*, 1973; *Maynard et al.*, 1983; *Baumjohann et al.*, 1985]. Intense electric fields (several millivolts per meter) have also been detected in the inner magnetosphere at $L$=2–5 during increased geomagnetic activity [*Pedersen*, 1992; *Maynard et al.*, 1996; *Rowland and Wygant*, 1998; *Wygant et al.*, 1998]. In general, the electric field usually displays a very complicated and variable behavior, where the fluctuations can be an order of magnitude larger than the mean value [*Mozer*, 1973]. Because such variable fields are difficult to include in models, there are many unresolved questions concerning the structure of the electric field that allows the formation of the observed intense nose structures.

In our paper we study a class of nose events seen as an overlapping of the plasma sheet (10–50 keV) and radiation belt populations at $L$=4–6 in the $H^+$ and $He^{++}$ spectrograms from the Polar Charge and Mass Magnetospheric Ion Composition Experiment (CAMMICE)/Magnetospheric Ion Composition Sensor (MICS) instrument. We called them "intense nose events" to stress that it is the large intensity (high fluxes, $>10^6$ (s cm$^2$ sr keV)$^{-1}$) that actually distinguish them. They penetrate deeply into the inner magnetosphere (with edges at $L$=3–4) within a relatively short period of time. Such high fluxes in the nose structures were also observed by Explorer 45 [*Ejiri et al.*, 1980] for storm time periods, whereas we observe intense nose structures even during relatively small substorms (see below). Furthermore, the observations are different in that Explorer 45 was in the equatorial plane, whereas Polar crosses the ring current region covering all latitudes from the equatorial plane to the lobe. Polar crosses both the ring current and near-Earth plasma sheet regions every 9 hours and spends a good portion of the time in the region of interest ($L < 6$). We examined observations from the entire year of 1997 and found about 400 intense nose structures, covering the entire range of MLT values and a wide spectrum of auroral electrojet ($AE$) values. We present statistical results of the occurrence and penetration of intense nose structures in the inner magnetosphere and their dependence on MLT and substorm activity level. In one well-observed event on November 3, 1997, we use three subsequent inner magnetosphere crossings by Polar and Interball Auroral probe on which we see the clear signatures of intense nose structures. We employ magnetic field modeling to examine the inward motion of the structure. In the discussion section, we deduce, by using the observed plasmapause position and particle tracing, the large-scale electric field which was required to explain the observed inward motion. We demonstrate that the inward displacement of the intense nose structure in this case could not be explained only by a large-scale electric field action, but requires very intense local electric fields in the near tail at $L$=4–5.

## 2. Instrumentation: Polar CAMMICE/MICS

The Polar spacecraft is on a ~86° inclination elliptical orbit with a 9 $R_E$ apogee, 1.8 $R_E$ perigee, and 18-hour orbital period. The orbit apogee is over the northern polar region. The spin axis is normal to the orbit plane to allow the imagers to view the high-latitude regions almost continuously and to enable the particle instruments to map the complete charged particle distribution function, including the loss cone.

The Charge and Mass Magnetospheric Ion Composition Experiment on board Polar was designed to measure the charge and mass composition of particles within the Earth's magnetosphere over the energy range of 6 keV/$Q$ to 60 MeV/$Q$ [*Wilken et al.*, 1992]. CAMMICE consists of two types of sensor systems: the Magnetospheric Ion Composition Sensor and the Heavy Ion

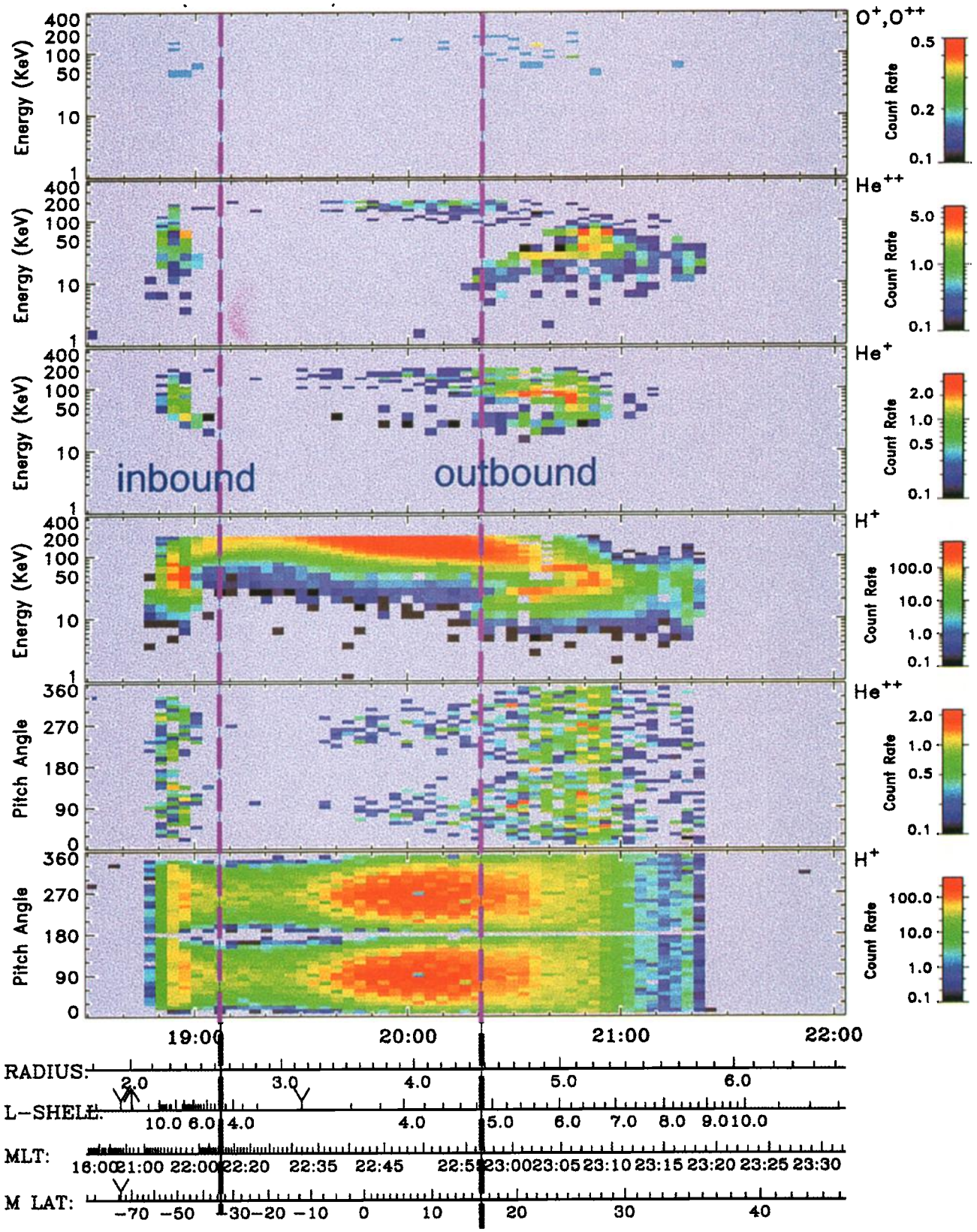


**Plate 1.** Time-energy spectrograms from Polar CAMMICE/MICS instrument on November 3, 1997, for $O^+$, $O^{++}$, $He^{++}$, $He^+$ and $H^+$. (bottom) Time-pitch angle spectrograms for $He^{++}$ and $H^+$. The edges of the intense nose structure for the inbound and outbound crossings are marked with vertical lines.

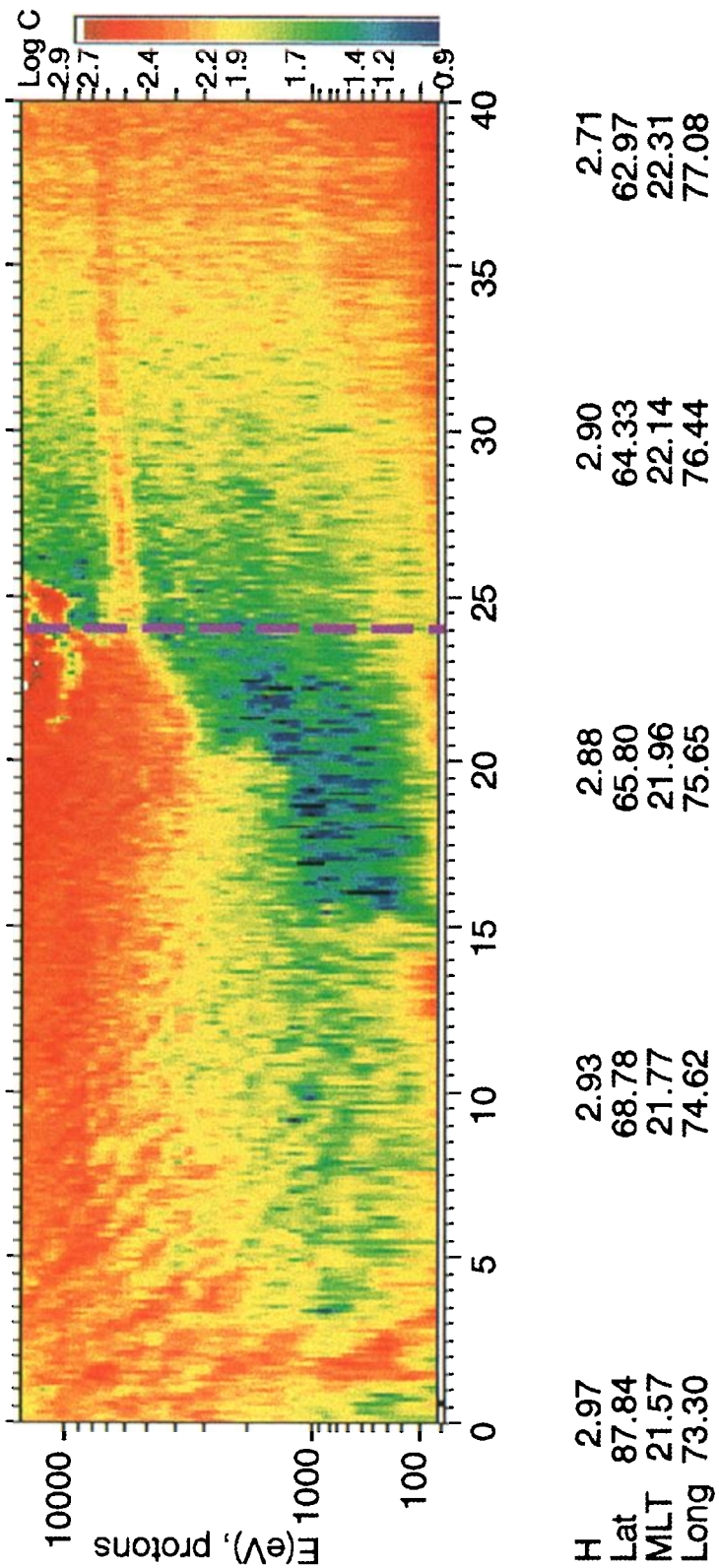


**Plate 2.** Energy-time spectrogram from the ION instrument on board the Interball Auroral spacecraft on November 3, 1997, beginning at 1600 UT. The edge of the intense nose structure is marked with a vertical line.

Telescope. The MICS sensor identifies each ion from measurements of time of flight, energy per charge, and total energy. An electrostatic analyzer allows entry of the ions in one of 32 energy/charge steps in the range of 10–200 keV/$e$. The ion energy is then increased by a postacceleration voltage of 22.4 kV/$Q$ to improve the efficiency at low energies. The particle events are analyzed on board to obtain their mass and mass/charge. The counts of the major ion species are accumulated into scalers, with a full 32-channel energy spectrum being telemetered once every 202 s. These measurements are used here to study the temporal and spatial properties of the ion populations in the inner magnetosphere.

## 3. Intense Nose Event on November 3, 1997

The intense nose structure observed on November 3, 1997, is a typical example of the events we selected for our study from the Polar/MICS measurements. In particular, this event was chosen for detailed examination, because the intense nose structure appeared as a result of an isolated substorm following a long period of very low activity. Furthermore, the Interball Auroral spacecraft crossed the same MLT sector 2 hours before the Polar measurements were made, which gave a unique chance to study the temporal evolution of the intense nose structure. The top panel of Figure 1 shows the

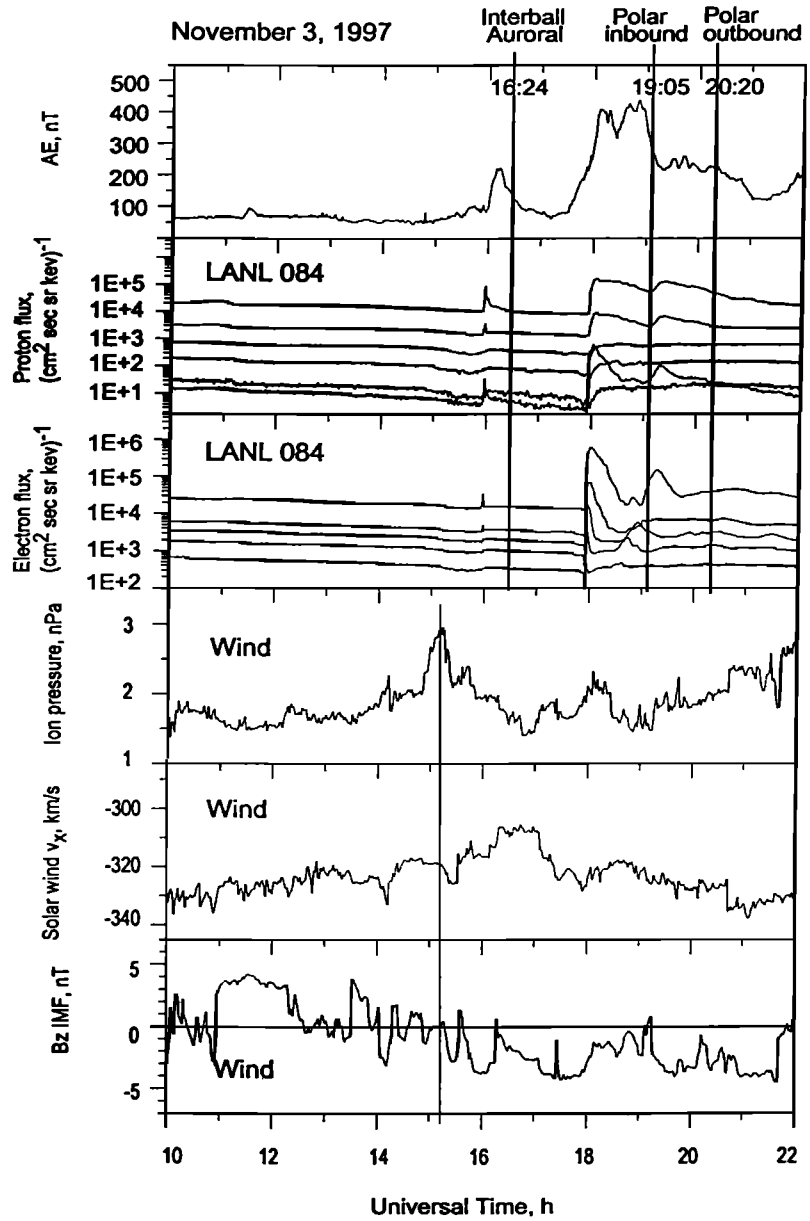


**Figure 1.** Overview of the solar wind and magnetospheric conditions on November 3, 1997. From top to bottom: preliminary $AE$ index; energetic proton and electron fluxes from LANL 1994-084; solar wind pressure, velocity $V_x$, and interplanetary magnetic field $B_z$ from Wind. In the top three panels, the vertical lines indicate the times when the Interball Auroral and Polar spacecraft traversed through the inner edge of the intense nose structure. In the lower panels, the vertical line marks the maximum of the pressure pulse in the solar wind.

$AE$ index for this event. Starting from 0200 UT on November 2, 1997, there was a very quiet period until about 1500 UT on November 3, 1997. The first (very modest) substorm onset was recorded at 1600 UT with $AE_{max} = 200$ nT at 1615 UT. There was a second (more pronounced) intensification at 1725 UT with $AE_{max} =$ 400 nT at about 1800 UT. The times when the inner edges of the intense nose structures were observed are shown by the vertical lines. The planetary activity index $Kp$ during these intensifications was about 2.

The next two panels in Figure 1 show energetic particle measurements from the Los Alamos National Laboratory (LANL) 1994-084 synchronous orbit particle analyzer, which measured electrons and ions in the energy range from 50 keV to 400 keV. The satellite was near midnight at 1700 UT. Around 1600 UT the proton and electron data show a very slight signature of a flux enhancement at lower energies. At 1755 UT a more pronounced injection was observed.

Interplanetary magnetic field (IMF) and solar wind plasma data from Wind showed that the solar wind was variable prior to the first intensification (Figure 1, lower panels). There was a distinct pressure pulse around 1515 UT concurrent with southward excursions of $B_z$. After 1500 UT, $B_z$ remained southward until 2200 UT. Wind was located at (110 $R_E$, -48 $R_E$, 32 $R_E$) at 1530 UT. Using the solar wind velocity ($V_x = -320$ km/s) gives a solar wind travel time to the subsolar point of about 37 min. Hence the pressure pulse (marked in the figure with the vertical line) reached the magnetopause a few minutes before 1600 UT and might have acted as a trigger for the first auroral activation.

Plate 1 shows the Polar CAMMICE/MICS measurements of count rates with time resolution of 202 s from the nightside magnetosphere during 1845–2125 UT. Because the nose structure is more clearly seen in the plot showing count rates, that is what is plotted in Plate 1. The intense nose-like structure (highest particle fluxes reached $10^6$ (s cm$^2$ sr keV)$^{-1}$) appeared clearly distinct from the ring current population in the $H^+$ energy spectrogram, and the lower-energy population continued to the nightside plasma sheet population at higher $L$ values. Clear signatures of the high-energy part of the intense nose structure can be seen in the energy range of 20-50 keV. The simultaneous fast plasma analyzer HYDRA measurements (data not shown) for ions and electrons with energies from 2 eV to 35 keV [*Scudder et al.*, 1995] complete the low-energy portion of the intense nose structure seen in the MICS data.

These observations allow us to conclusively determine that this event was an intense nose event. During the outbound pass, the inner edge of the intense nose structure was observed at 2020 UT at 2256 MLT and at $L = 4.8$. The same intense nose structure (as it will be argued in more detail below) was also seen during the preceding inbound pass of Polar. The MICS data with 32.5-s resolution (data not shown) was used to determine the intense nose edge position at 1905 UT to be at 2212 MLT and at $L = 4.6$.

For the heavier ion species, we note that only the $He^{++}$ spectrogram shows similar signatures of an intense nose-like structure in the same energy range of 20–50 keV. The position of the intense nose edge in $He^{++}$ is close to that seen in the $H^+$ spectrogram. The energy thresholds for the ion measurements are 15 keV for $H^+$, 8 keV for $He^{++}$, 30 keV for $He^+$, and 70 keV for $O^+$ and $O^{++}$. Therefore we cannot draw conclusions of the intense nose-like signatures in the $He^+$ and $O^+$ spectrograms. The existence of $He^{++}$ ions indicates that the plasma within the nose structure was at least partly of solar wind origin.

The Interball Auroral probe has a perigee at 770 km, an apogee at 20,000 km and a 65° inclination. The spacecraft crossed the inner magnetosphere field lines from high to low latitudes during 1600-1640 UT in the same local time sector with Polar (around 2200 MLT). Plate 2 shows an energy-time spectrogram from the Ion instrument [*Sauvaud et al.*, 1998] performing measurements in the energy range from 10 eV to 20 keV. A bright structure is observed in the energies higher than about 3 keV at 1610-1624 UT, which we associate with the same intense nose structure as seen by Polar a few hours later. The edge of this intense nose-like structure is observed at 1624 UT.

Thus for the November 3, 1997, event we have three consecutive measurements of the edge positions of the intense nose structures made by the Polar and Interball Auroral satellites. We utilize an event-oriented magnetic field modeling technique [see *Kubyshkina et al.*, 1999] to deduce the equatorial crossing points of the field lines where the inward edge of the intense structure is observed ($R_{eq}$). The magnetic field model used was the Tsyganenko 1996 version [*Tsyganenko*, 1995], which takes the tilt angle, solar wind dynamic pressure $P_{SW}$, IMF $B_Y$ and $B_Z$, and the $Dst$ index as input. If one uses the measured solar wind and IMF values and the observed value of $Dst$, the model field does not give good agreement with the magnetic field measurements made on board Polar (which were notably variable during 1500-1700 UT). Therefore the large parameter range was explored for each of the input parameters ($P_{SW}, B_Y^{IMF}, B_Z^{IMF}$, $Dst$) to find the parameters that would give the best fit to the local field measurements at each time step separately and to the isotropic boundary measurements recorded by the DMSP spacecraft (for details, see *Kubyshkina et al.* [1999]). The best fit parameters were found to be $P_{SW} = 2.0$ nPa, $Dst = 10$ nT, $B_Y^{IMF} = 7.0$ nT, and $B_Z^{IMF} = 0.0$ nT (see Figure 2 (left)).

Figure 2 (right) shows the Polar and Interball Auroral footpoints (solid curves) as a function of time mapped to the equatorial current sheet. Solid vertical lines with triangles give the times of the intense edge crossings (marked on the spacecraft trajectory) by both spacecraft. Solid vertical lines with circles indicate the Polar crossings of the plasmapause. Table 1 presents a summary of the edge positions of the three intense nose structures as seen by Polar and Interball Auroral. Fig-

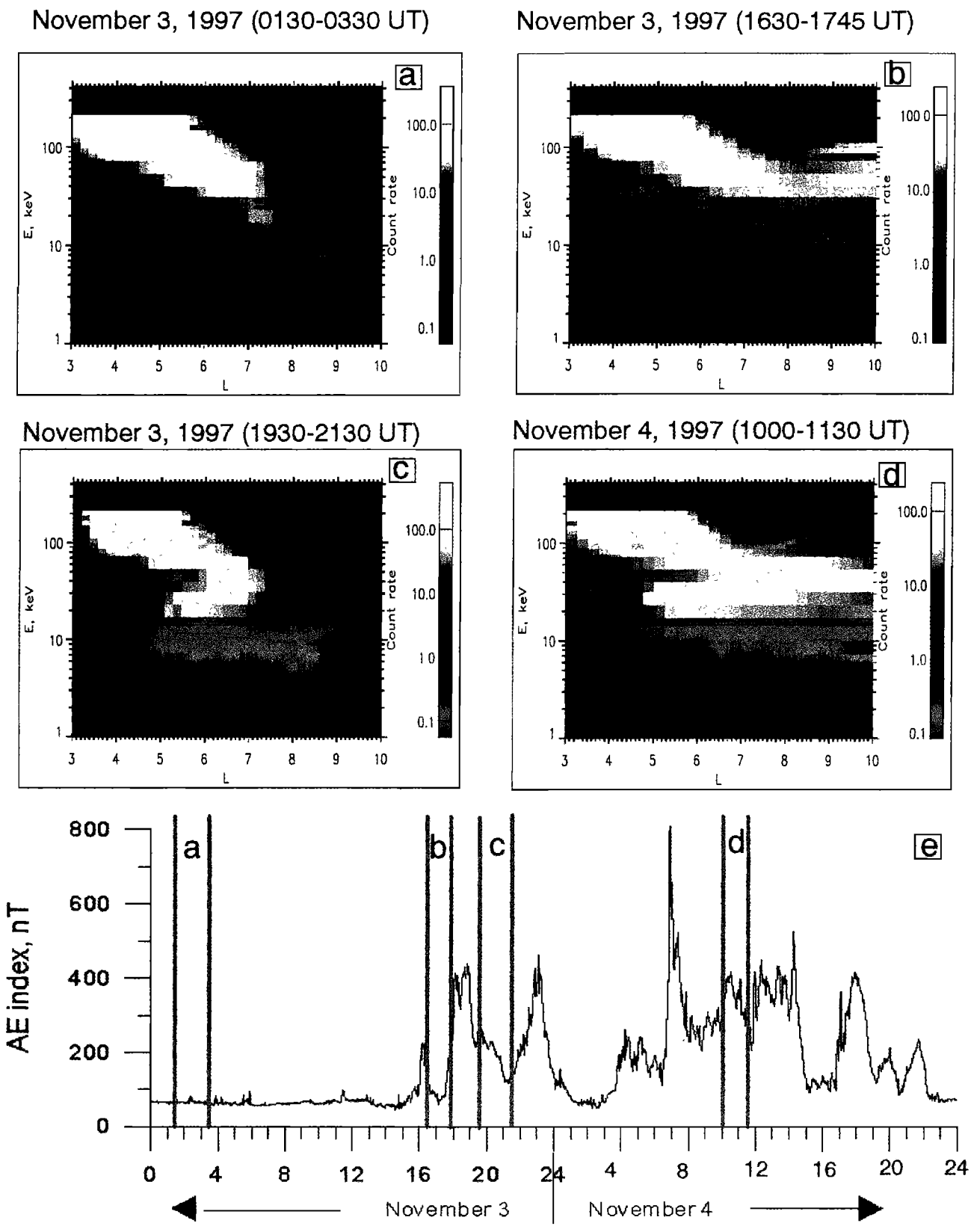


**Plate 3.** (top) Time evolution of the intense nose structure on November 3–4, 1997. (a) Quiet period, no nose structure; (b) quiet period, no nose structure; (c) initial observation of the nose structure; (d) nose structure present. The vertical lines mark the inner edges of the intense nose structures. (bottom) *AE* index for November 3–4, 1997. The vertical lines mark the times when Polar passed through the inner magnetosphere.

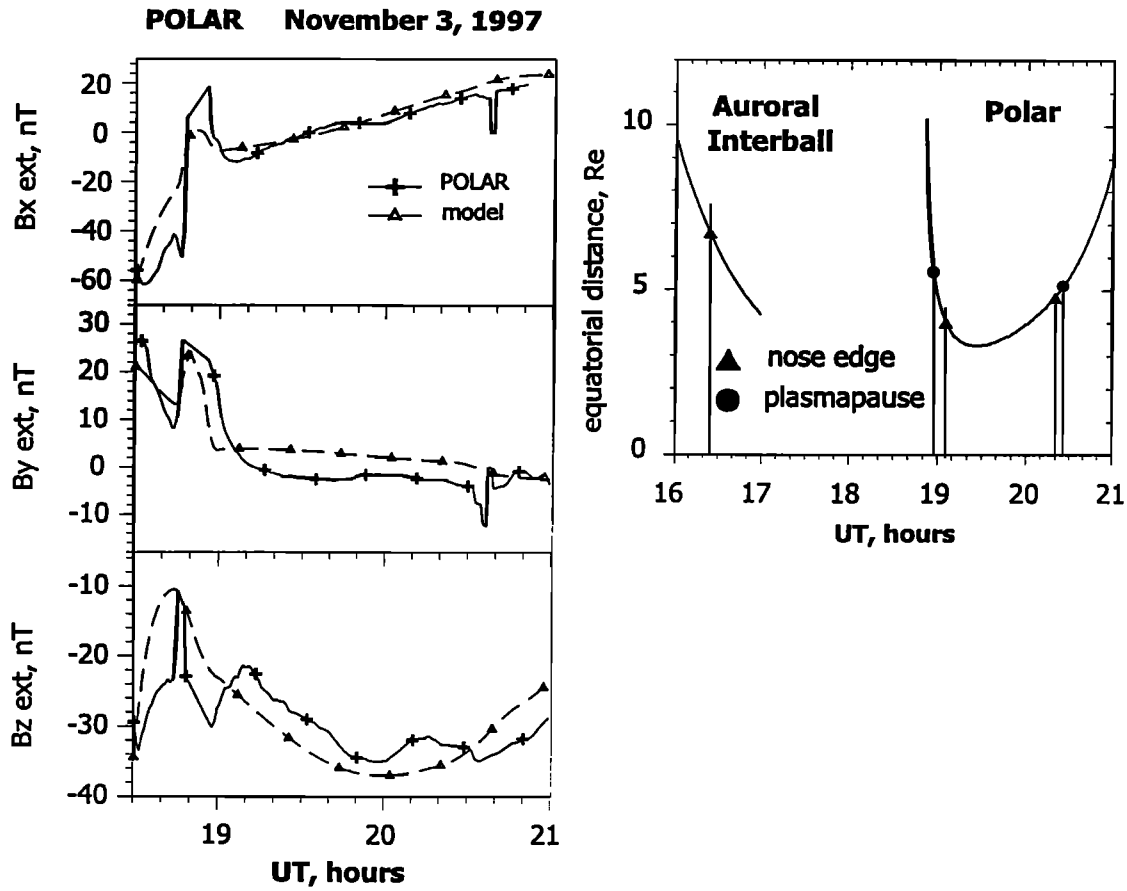


**Figure 2.** Magnetic field modeling results for November 3, 1997. (left) Magnetic field measurements from Polar (solid line, crosses) and magnetic field model (dashed line, triangles). (right) Footpoints of the Polar and Interball Auroral spacecraft (solid curves) mapped to the equatorial plane as a function of time. The solid lines with triangles mark the nose edge locations. The solid lines with circles show the plasmapause location.

ure 2 (right) indicates that the equatorial distances of the intense nose edges during the inbound (1905 UT, high magnetic latitudes) and outbound (2020 UT, low magnetic latitudes) Polar passes are very close (4.7 $R_E$ and 4.86 $R_E$). Thus we conclude that Polar detected the same intense nose structure twice. The nose edge positions during both Polar passes are the same within the accuracy of the model mapping.

Plate 3 illustrates the time evolution of the intense nose structures. Consequent $L$ spectrograms for $H^+$ are shown for November 3, 1997, when Polar was (Plate 3a) near midnight (0130–0330 UT), (Plate 3b) near noon (1630–1745 UT), (Plate 3c) near midnight (1930–2130 UT), and for November 4, 1997, when Polar was (Plate 3d) near noon (1000–12130 UT). The spectrograms in Plates 3a and 3b were recorded during the quiet period (see Figure 1), and there are no signatures of the intense nose-like structure. The intense nose structure in Plate 3c is the one described in detail above. A similar intense nose-like structure was observed on the dayside (Plate 3d). Polar measured this structure about 14 hours later than that on the nightside. After the second substorm on November 3, 1997, there were additional disturbances, and November 4, 1997, was a disturbed day. Therefore we cannot conclusively relate these structures seen on the nightside and on the dayside about 14 hours apart.

**Table 1.** Positions of the Inner Edges of Three Consecutive Intense Nose Structures on November 3, 1997

| Satellite | Time, UT | $R_{eq}$, $R_E$ | MLT |
|---|---|---|---|
| Interball Auroral | 1624 | 6.73 | 2200 |
| Polar/inbound | 1905 | 4.7 | 2212 |
| Polar/outbound | 2020 | 4.86 | 2256 |

## 4. Statistical Results

### 4.1. MLT and Activity Dependence of Intense Nose Events

Polar crosses the auroral flux tubes at varying latitudes, but the analysis here was limited to crossings

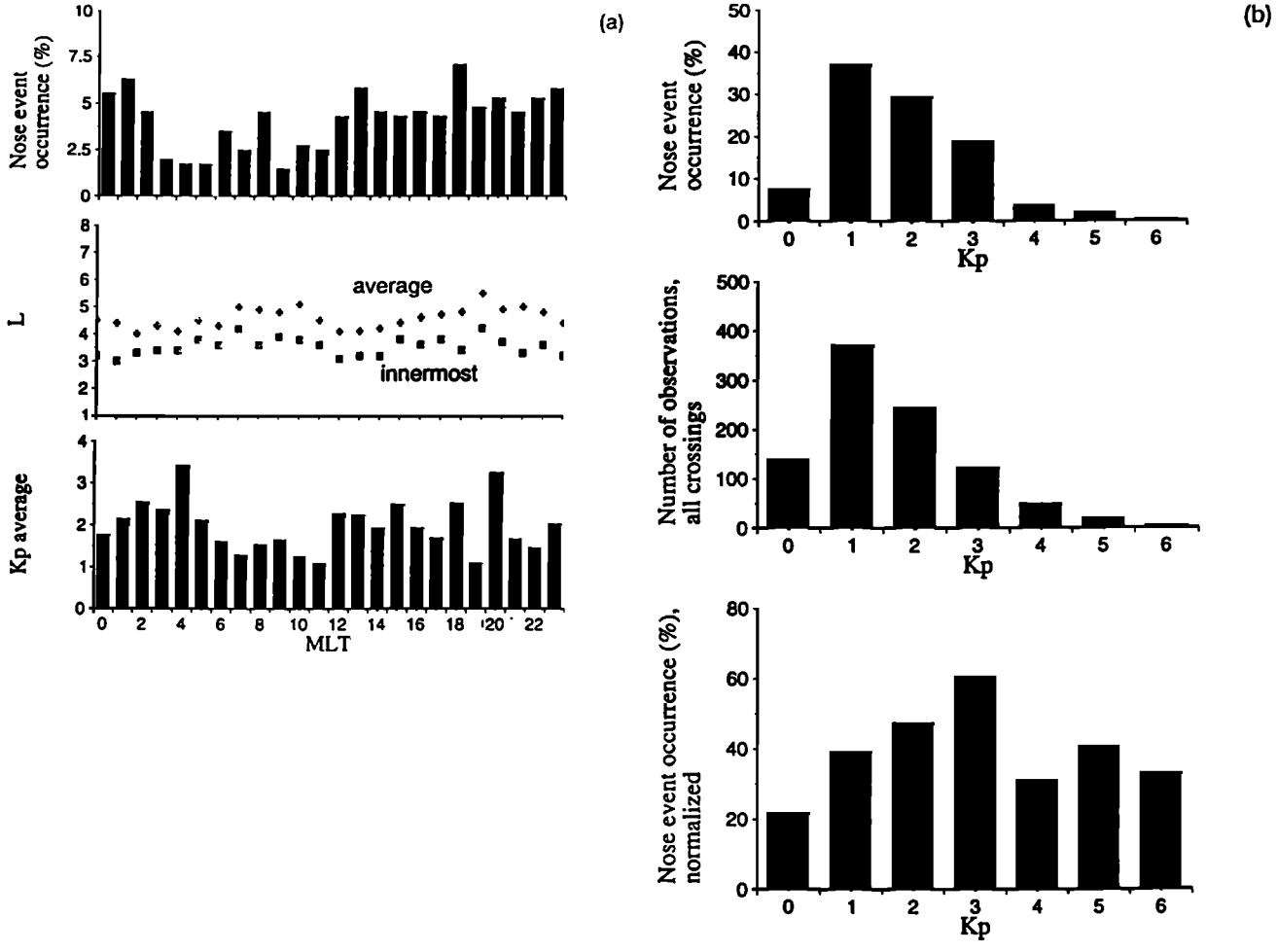


**Figure 3.** Statistical results of intense nose structures. (a) (top) Occurrence frequency of intense nose structures normalized to the total number of events as a function of magnetic local time. (middle) Average and smallest $L$ values of the inner edges of the intense nose structures as a function of magnetic local time. (bottom) Average of $Kp$ during all crossings during 1997 when nose structures were observed as a function of magnetic local time. (b) (top) Occurrence frequency of intense nose structures as a function of $Kp$. (middle) Number of observations during all crossings during 1997 as a function of $Kp$. (bottom) Occurrence frequency of intense nose structures normalized by the number of $Kp$ observations during all crossings as a function of $Kp$.

at low magnetic latitudes, <30°–40°, where the structure is better resolved. We have analyzed the MICS measurements for the year 1997, during which Polar completed a full rotation around the Earth visiting all MLT sectors twice. From all crossings, 396 events were selected to be intense nose events, with signatures such as those shown in the case study above.

The top panel of Figure 3a shows the occurrence of intense nose structures normalized by the total number of events (396) as a function of different MLT sectors. In general, fewer intense nose-like events are observed near dawn than near dusk. There were distinct peaks near midnight and noon as well as near 1800 MLT, but the structures were observed in all local time sectors.

For the same data set, the $L$ values of the inner edge of the intense nose structure were determined. The middle panel of Figure 3a shows the inner edge locations ($L$ values) of the intense nose structures as a function of MLT. Squares correspond to the innermost $L$ value in the data set, and crosses show the average $L$ for all intense nose events observed at that MLT sector. The intense nose structures penetrate deepest around midnight (innermost $L = 3$) and noon ($L = 3.1$). Average $L$ values show the same tendency: $L = 4$ and $L = 4.1$ for midnight and noon, respectively. The intense nose structures were observed at slightly lower $L$ near dusk (innermost $L = 3.4$) than near dawn ($L = 3.6$).

As the intense nose structures appear during geomagnetically disturbed periods, it is possible that their formation is related to the substorm-associated processes. In order to relate the intense nose structures with the level of geomagnetic activity, each event was tagged with the $Kp$ index preceding the observation period. The $Kp$ index was used because of the long lifetime of the nose structures and the long orbital period of Polar, which do not allow for detailed timing of the formation

of the intense nose structures. To check if the above local time distributions are affected by the average level of activity when Polar visited different local time sectors, the bottom panel of Figure 3a presents the average $Kp$ values for every MLT sector. These average values were computed by using $Kp$ values during passes that Polar made during 1997 in that particular local time sector when nose events were observed. Note that there is no correlation between the number of the observed intense nose events or their inner edge $L$ value with the $Kp$ value at any given MLT sector (correlation coefficient is about 0.11).

The upper panel of Figure 3b presents the dependence of the intense nose structure occurrence on the $Kp$ index. A steep increase of the occurrence frequency is found even with minor increase of $Kp$ to $Kp = 1$. The decrease of the number of events with the subsequent $Kp$ growth to larger values can be caused by the event selection criteria: Only events with clear intense nose signatures were accepted as intense nose events. During high magetic activity the magnetosphere is more disturbed and the signatures are not as clear, and therefore it is difficult to resolve the intense nose structures.

Again, in order to examine the effect independent of the $Kp$ distribution throughout the year of 1997, we plot in the middle panel of Figure 3b the total number of Polar crossings as a function of the $Kp$ values during the crossings. The most common value of $Kp$ was around 1, with a smooth decrease in the number of events as $Kp$ increases. The bottom panel of Figure 3b shows the occurence of intense nose events as a function of $Kp$ normalized by the total number of crossings made at any given $Kp$ value. This normalized figure shows that the number of intense nose events increases with increasing $Kp$ up to $Kp = 3$ and, then, starts to decrease, which may again be caused by the event selection criteria. By normalization we remove the biasing effects of $Kp$ occurrence (less events with higher $Kp$), and the data set still shows the clear tendency to increase the number of events for higher $Kp$ values.

### 4.2. Dependence of the Intense Nose Structure Inner Edge on Substorm Activity

The dependence of the location of the inner edge of the intense nose structure on substorm activity was examined by selecting isolated substorms that were preceded by at least 1 day of magnetic quiescence. This allowed us to conclusively associate the substorm activity with the intense nose structure formation. From Polar MICS measurements made in 1997–1999, 24 events met our selection criteria. There are no clear signatures of intense nose structures during extended quiet periods. Figure 4 gives the dependence of the edges of the intense nose structures ($L$ values) on the level of the preceding substorm activity (maximum of $AE$). Note that the intense nose-like structures are observed not only during pronounced activity, but also during relatively small disturbances ($AE$ of 150–250 nT). Figure 4 also shows a tendency of particles to penetrate closer to the Earth as the level of substorm activity increases.

## 5. Discussion

In this paper, we have shown observations of intense nose structures measured twice by Polar and once by Interball Auroral within 4 hours. Here we discuss the large-scale convection pattern during those observations and whether that convection would be sufficient to bring the plasma sheet population deep into the inner magnetosphere.

### 5.1. November 3, 1997 Event

**5.1.1. Plasmapause position.** The large-scale electric field can be examined by using the observations of the cold plasma population, especially the plasmapause positions as measured by Polar. The times and positions of the plasmapause crossings during November 3, 1997, were determined from the saturation points of the spacecraft electric potential using the high-resolution Polar EFI data [*Harvey et al.*, 1995]. The equatorial

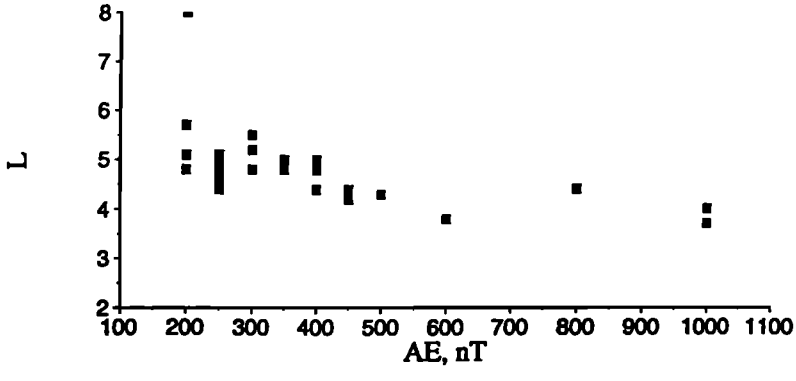


**Figure 4.** Location of the inner edge of intense nose structure ($L$ values) as a function of substorm activity ($AE$ index).

**Table 2.** Observation Times and Positions of the Plasmapause on November 3, 1997

| Plasmapause Position | Time, UT | $R_{eq}$, $R_E$ | MLT |
|---|---|---|---|
| PP1 | 1857 | 5.58 | 2148 |
| PP2 | 2025 | 5.195 | 2254 |

projections of the plasmapause positions were computed by using the magnetic field model described above and are shown in Table 2 for the inbound (PP1) and outbound (PP2) Polar passes. The actual plasmapause did not move between inbound and outbound passes of Polar. The slight difference in plasmapause location comes from the different local time of the measurements (it is consistent with, for example, *Ejiri et al.* [1980]).

Figure 14 of *Ejiri et al.* [1980] is reproduced here as Figure 5, and shows the time-evolving positions of ions and electrons in the energy versus $L$ coordinates in the equatorial plane for MLT = 2400 and MLT = 2100. The calculations of *Ejiri et al.* [1980] were made by assuming that a continuous particle source at all times was located at $L = 10$ and 2000–0400 MLT, for all energies and pitch angles. No local energization processes or loss mechanisms were considered. *Ejiri et al.* [1980] traced particles in a dipole magnetic field together with a Volland-Stern type convection electric field taking into account also corotational electric field. In the Volland-Stern convection electric field model, the large-scale potential is given by $\Phi = AR^{\gamma} \sin\phi$, where $A$ is the coefficient which determines the electric field and $\phi$ is the local time. Using this electric field model with $\gamma = 2$ was successful in interpreting the locations of the plasmapause observed by Explorer 45 (see, for example, references in the work of *Ejiri et al.* [1980]). For $\gamma = 2$, $A$ is given as a function of $Kp$ by

$$A = 0.045/(1 - 0.159Kp + 0.0093Kp^2)\ \text{kV}/R_E^2. \quad (1)$$

On the other hand, the relation of the coefficient $A$ with the stagnation point $L = L_0$ at dusk for zero-energy particles is

$$L_0 = 3.6/[A(\text{kV}/R_E^2)]^{1/3}. \quad (2)$$

These equations now determine the stagnation point location for a given level of magnetic activity. The computations in Figure 5 were done by using $\gamma = 2$ and $A = 0.057\ \text{kV}/R_E^2$, which corresponds to an activity level of $Kp = 4+$.

*Ejiri et al.* [1978] used the plasmapause position measured by Explorer 45 to determine the best fit convection electric field model ($A$ value) in the Volland-Stern formulation. In Figure 5, the plasmapause position labeled by arrow P is at about 3.9 $R_E$ at 2100 MLT and at 3.3 $R_E$ at 2400 MLT, when the stagnation point was $L_0 = 5$. If we interpolate linearly to 2200 and 2300 MLT to correspond to the November 3, 1997, observations, we get 3.7 $R_E$ and 3.5 $R_E$, respectively. If we

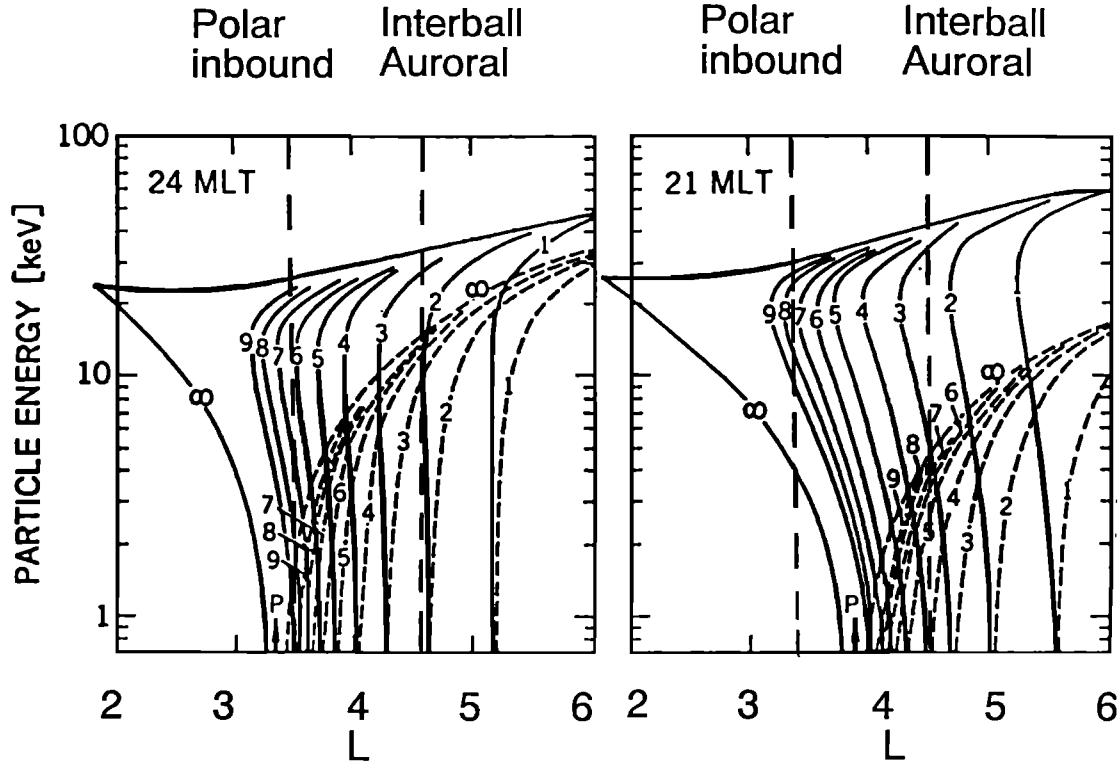


**Figure 5.** Time evolution of the positions for ions and electrons in energy versus $L$ coordinates in the equatorial magnetosphere for (left) 2400 MLT and (right) 2100 MLT [after *Ejiri et al.*, 1980].

change the intensity of the convection electric field represented in terms of $L_0$, the indicated energy and radial distance scales change by factors $5/L_0$ and $L_0/5$, respectively. Scaling the interpolated Figure 5 to adjust it to the observed plasmapause position at 5.2 $R_E$, we obtain a stagnation point $L_0 \sim 7.4$. For this stagnation point, equation (2) gives a value for the coefficient $A = 0.115$ kV/$R_E^2$.

On the other hand, using equation (1) and the observed $Kp = 2$, one obtains a value $A \sim 0.12$ kV/$R_E^2$. This value of $A$ corresponds to an electric field $E_y = -d\Phi/dy = AR + Ay^2/R$, which gives $E_y \sim 0.1$ mV/m at midnight at $L = 5$. This is a typical and probable estimate of the actual average electric field during the period when both the plasmapause and intense nose structure were observed. Because the value determined by using the *Ejiri et al.* [1980] results in the infinitely long time limit and the value determined from the observed plasmapause position agree, we argue that the plasmapause in this event could be formed under a convection electric field of the Volland-Stern type with a value of about 0.1 mV/m. Plasmaspheric ions are slowly corotating with the Earth, and hence the plasmapause location depends on the history of the convection electric field variations rather than on the instantaneous value of this field.

**5.1.2. Formation of intense nose structures.** As is seen from the Polar observations of the intense nose structure edges (Table 2), the intense nose structure was observed to be 0.4–0.6 $R_E$ inside the plasmapause. The ordinary nose structure may be formed in the stationary large-scale electric field after a long time with corresponding losses with the edge, for example, at $L = 3$, but the intensity is too small to determine the structure on the CAMMICE/MICS energy-time spectrograms. Assuming that the plasmapause was formed in the weak electric field (0.1 mV/m) estimated above, we now consider whether the intense nose structure could also be formed under the influence of this convection electric field.

The Interball Auroral measurements show that the inner edge of the intense nose structure was 2 $R_E$ outward of the plasmapause (at 1624 UT, it was at 6.73 $R_E$). Thus there was no indication of plasma sheet-like plasma earthward of the intense nose edge at that time. Therefore the intense nose edge position recorded by Interball Auroral gives us the closest possible location of the plasma population that could form the intense nose structure observed during the Polar inbound pass (intense nose edge at 4 .7 $R_E$) 2.5 hours later. The injection event registered at 6.6 $R_E$ by the LANL satellite at 1755 UT was the first indicator of intense inward plasma trasport connected with the substorm intensification at 1725 UT. After this, the intense nose structure moved inward by 2 $R_E$ during only about 1 hour.

As particles with smaller pitch angles can come closer to the Earth along magnetic field lines, there is some concern that measurements made at different magnetic latitudes might not give a similar picture of the same structure. Polar at 1900 UT was at about the same distance and magnetic latitude as Interball Auroral. Comparison of the Polar observations during the auroral zone crossing at high magnetic latitudes and, later, at low latitudes confirms that the innermost boundary of the intense nose structure was located on the same field line for different pitch angles. This implies that the difference between the intense nose structure positions observed by Interball Auroral (1624 UT) and later by Polar should be interpreted as the result of fast transport rather than an effect of different pitch angles being sampled.

The Polar HYDRA data indicate that the lowest-energy electron intense nose boundary approximately coincides with the ion boundary. This boundary can therefore be interpreted as the innermost boundary of zero-energy population coming from the plasma sheet. Thus we can scale Figure 5 to adjust it to the observed intense nose edge positions. Even crude estimates show that it takes about 5 hours to move the intense nose edge from 6.73 $R_E$ to 4.7 $R_E$ with the electric field determined above. The observed inward shift (2 $R_E$ in 1 hour) therefore cannot be explained by the cross-tail electric field (0.1 mV/m at 5 $R_E$). Thus to get the observed high ion fluxes transported requires strong electric fields acting upon the plasma population, much higher than those estimated from the plasmapause location. Such electric fields can be local and inductive. Scaling the $E - L$ diagrams in Figure 5 gives $E_y >$ 1 mV/m as a lower estimate of the electric field needed to shift the intense nose structure by 2 $R_E$ in less than 1 hour. Higher electric fields would give even more rapid convection times.

Such intense electric fields are not uncommon in the inner magnetosphere during substorm expansion phases [*Maynard et al.*, 1996]. *Rowland and Wygant* [1998] reported the presence of spatially localized enhancement of the large-scale electric field at $3 < L < 6$ ($E_y \sim 1.0$ mV/m), but only during a high level of magnetic activity ($Kp > 3$). In the event shown here, $AE$ was very moderate and $Kp$ was around 2, and hence one would not expect a strong large-scale electric field enhancement in the inner magnetosphere. We suggest that such structures are formed by short-lived impulsive electric fields that are also associated with the energetic particle injections at geosynchronous orbit even during moderate activity. The suggestion that the particles are injected into the inner magnetosphere from the near-Earth plasma sheet by a strong inductive electric field due to a substorm dipolarization was used by *Ebihara et al.* [1999] in their computer simulation for the motion of energetic trapped particles during a magnetic storm.

### 5.2. Polar Particle Observations in the Inner Magnetosphere

It has been proposed that the intense nose structures seen in the ion spectrograms at $L$=4–6 (even inside the

plasmapause) are formed as a result of inward plasma convection [*Smith and Hoffman*, 1974; *McIlwain*, 1972; *Ejiri et al.*, 1980; *Kistler et al.*, 1989; *Sergeev et al.*, 1991, 1998; *Shirai et al.*, 1997; *Fennell et al.*, 1998; *Peterson et al.*, 1998]. We searched through the Polar MICS data during 1996-1999 together with concurrent LANL geosynchronous proton and electron data near midnight. The injection times as registered at 6.6 $R_E$ were determined and compared with the observation times of the inner edges of intense nose-like structures during isolated substorms. It was found that in each case, the intense nose structures were preceded by an injection event registered at 6.6 $R_E$. The shortest time between the geostationary orbit injection and MICS intense nose event observation was 25 min, which is consistent with the results by *Ejiri et al.* [1980]. Therefore we associate the formation of the intense nose structures with substorm onsets and conclude that these structures can form within about 25 min of the substorm onset. Assuming that there was no preexisting plasma population at $L$=4–6 before the substorm, this would again imply very rapid transport of plasma sheet plasma from beyond geosynchronous orbit to the inner magnetosphere.

*Fennell et al.* [1998] studied another class of events, multiply peaked ion spectra that appear as traces extending from large to small $L$ values. These structures are seen in all major energy species, and they occur near 10–20, 30–50, and 90–120 keV. *Fennell et al.* [1998] also concluded that drift calculations can account for only some but not all properties of the traces. In addition to differences in the spectral shape between the peaked structures and intense nose events, they also differ in the plasma composition: whereas the peaked structures show strong indications of ionospheric material ($He^+$, $O^+$), the intense nose events also show a plasma component originating from the solar wind ($He^{++}$). However, because the MICS measurements have quite high energy thresholds for the ionospheric species, this conclusion warrants further study. Also the abundance of ionospheric ions in the inner magnetosphere is proportional to the level of geomagnetic (substorm or storm) activity [*Daglis et al.*, 1994].

Our statistical study showed that, in general, fewer intense nose-like events were observed at dawn than at dusk, which is consistent with previous observations made by *Ejiri et al.* [1980]. However, the results show some differences with the preliminary statistics of *Fennell et al.* [1998]. They found that the occurrence frequency of the spectral peaks is largest on the dayside and smallest near midnight. Furthermore, for multiple traces the occurrence peaks on the dayside.

As was noted above, statistics of the intense nose structures revealed that they are associated with substorm activity (no events were found during quiet periods) but that a significant portion of the events occur during small to moderate activity (150– to 250–nT disturbance in the $AE$ index). Furthermore, the intense nose structures can live for more than a day in the inner magnetosphere after forming in the nightside. This life period was obtained for the events with the prolonged quiet period after the disturbance which could form the observed intense nose structure. But the exact lifetime of the events is difficult to define, because their lifetime is longer than the typical interval between two substorms. On the other hand, *Fennell et al.* [1998] observed the spectral peaks during enhanced magnetic activity or during the recovery phase. In either case, it seems clear that enhanced large-scale convection associated with high magnetic activity cannot alone account for their formation.

## 6. Conclusions

We have analyzed Polar CAMMICE/MICS measurements during 1997 by using the flux versus time spectrograms for different ion species to examine "intense nose structures," which are seen as strong enhancements of low-energy (plasma sheet-like) ions in the ring current region. In this paper we show statistical results of their occurrence, lifetime, inward penetration, and relation to substorm activity. The main results are summarized below:

1. Fewer intense nose events were observed in the dawn sector than in the dusk sector. This is probably due to the particle losses in the dayside magnetosphere (precipitation and charge exchange with exospheric neutrals) and due to the differences in the particle trajectories as particles drift around the Earth.
2. The intense nose structures recorded around midnight and noon were observed to reach closer to the Earth ($L$ = 3.1) than those recorded near dawn and dusk ($L$ = 3.5).
3. Intense nose structures can persist for more than 1 day in the inner magnetosphere.
4. There are no clear signatures of intense nose structures during long lasting geomagnetically quiet periods, but even small disturbances ($AE \sim$ 150–250 nT) increase their occurrence frequency considerably. The decrease in the number of events for $Kp > 3$ may be caused by selection criteria (during strongly disturbed conditions the nose structures are difficult to identify in the data).
5. Intense nose structures were already found 25 min after an injection registered at geosynchronous orbit. Such rapid formation of the nose structure is one piece of evidence that an enhanced large-scale convection electric field is not sufficient for the formation of the nose structures.

In a case study, we examined the time evolution of an intense nose structure that formed on November 3, 1997. We compared the nose structure location and the plasmapause location with drift trajectory computations by *Ejiri et al.* [1980]. The results are summarized below:

1. The plasmapause location was consistent with a large-scale Volland-Stern type weak electric field of about 0.1 mV/m. We conclude that the plasmapause probably formed at that distance during the long quiet period preceding the nose structure formation.
2. Three consequent observations of the intense nose structure indicated an inward motion of about 2 $R_E$ during about 1 hour. Comparisons with the model calculations clearly indicate that much stronger electric fields ($E_y > 1$ mV/m) are required for this inward motion. These electric fields may be local and they most likely are inductive. We suggest that the nose events are formed by the intense and highly variable electric fields that are formed in connection with substorm onsets, but further analysis is left for a future study.

**Acknowledgments.** We thank World Data Center C2 for Geomagnetism, Kyoto, for the provisional *AE* index data used in this study. N. Ganushkina's work at Finnish Meteorological Institute is supported by the Academy of Finland. The work by N. Ganushkina was partly supported by grant N 11-1999 from the Russian Foundation of Perspective Researches and grant N 98-05-64508 from the Russian Foundation for Basic Research.

Michel Blanc thanks Masaki Ejiri and Ioannis Daglis for their assistance in evaluating this paper.

## References

Baker, D. N., T. I. Pulkkinen, V. Angelopoulos, W. Baumjohann, and R. L. McPherron, The neutral line model of substorms, *J. Geophys. Res., 101,* 12,975-13,010, 1996.

Baumjohann, W., G. Haerendel, and F. Melzner, Magnetospheric convection observed between 0600 and 2100 LT: Variations with *Kp*, *J. Geophys. Res., 90,* 393-398, 1985.

Daglis, I. A., S. Livi, E. T. Sarris, and B. Wilken, Energy density of ionospheric and solar wind origin ions in the near-Earth magnetotail during substorms, *J. Geophys. Res., 99,* 5691-5703, 1994.

Daglis, I. A., R. M. Thorne, W. Baumjohann, and S. Orsini, The terrestrial ring current: Origin, formation, evolution, and decay, *Rev. Geophys., 37,* 407-438, 1999.

Ebihara, Y., M. Ejiri, and H. Miyaoka, Enhancements of differential flux of energetic particles in the inner magnetosphere associated with a magnetic storm (extended abstract), *Proc. NIPR Symp. Upper Atmos. Phys., 11,* 150-153, 1998.

Ebihara, Y., M. Ejiri, and H. Miyaoka, Simulation on ring current formation: A case study of a storm on February 13, 1972, *Proc. NIPR Symp. Upper Atmos. Phys., 12,* 1-11, 1999.

Ejiri, M., Trajectory traces of charged particles in the magnetosphere, *J. Geophys. Res., 83,* 4798-4810, 1978.

Ejiri, M., R. A. Hoffman, and P. H. Smith, The convection electric field model for the magnetosphere based on Explorer 45 observations, *J. Geophys. Res., 83,* 4811-4815, 1978.

Ejiri, M., R. A. Hoffman, and P. H. Smith, Energetic particle penetrations into the inner magnetosphere, *J. Geophys. Res., 85,* 653-663, 1980.

Fennell, J. F., et al., Multiple discrete-energy ion features in the inner magnetosphere: Polar observations, in *Physics of Space Plasmas*, vol. 14 , MIT Center for Theor. Geo/Cosmo Plasma Phys., Cambridge, Mass., 1998.

Friedel, R. H. W., A. Korth, and G. Kremser, Substorm onsets observed by CRRES: Determination of energetic particle source regions, *J. Geophys. Res., 101,* 13,137-13,154, 1996.

Harvey P., et al., The electric field instrument on the Polar satellite, *Space Sci. Rev., 71,* 583-596, 1995.

Kistler, L. M., et al., Energy spectra of the major ion species in the ring current during geomagnetic storms, *J. Geophys. Res., 94,* 3579-3599, 1989.

Kubyshkina, M. V., V. A. Sergeev, and T. I. Pulkkinen, Hybrid input algorithm: An event-oriented magnetospheric model, *J. Geophys. Res., 104,* 24,977-24,993, 1999.

Maynard, N. C., T. L. Aggson, and J. P. Heppner, The plasmaspheric electric field as measured by ISEE 1, *J. Geophys. Res., 88,* 3991-4003, 1983.

Maynard, N. C., et al., Dynamics of the inner magnetosphere near times of substorm onsets, *J. Geophys. Res., 101,* 7705-7736, 1996.

McIlwain, C. E., Plasma convection in the vicinity of geosynchronous orbit, in *Earth's Magnetospheric Processes*, edited by B. M. McCormac, p. 268, D. Reidel, Norwell, Mass., 1972.

Mozer, F. S., Electric fields and plasma convection in the plasmasphere, *Rev. Geophys., 11,* 755, 1973.

Pedersen, A., Substorm electric and magnetic field signatures on GEOS-1, GEOS-2 and ISEE-1, in *Proceedings of the First International Conference on Substorms, Kiruna, Sweden, 23-27 March 1992, Eur. Space Agency Spec. Publ., ESA SP-335,* 237-241, 1992.

Peterson, W. K., et al., Imaging the plasma sheet with energetic ions from the Polar satellite, in *Substorms-4*, edited by S. Kokubun and Y. Kamide, pp. 813-816, Terra Sci., Tokyo, and Kluwer Acad., Norwell, Mass., 1998.

Rowland, D. E., and J. R. Wygant, Dependence of the large-scale, inner magnetospheric electric field on geomagnetic activity, *J. Geophys. Res., 103,* 14,959-14,964, 1998.

Sauvaud, J.-A., et al., The ION experiment onboard the Interball Auroral satellite; initial results on velocity-dispersed structures in the cleft and inside the auroral oval, *Ann. Geophys., 16,* 1056-1069, 1998.

Scudder, J., et al., Hydra – A 3-dimensional electron and ion hot plasma instrument for the Polar spacecraft of the GGS mission, *Space Sci. Rev., 71,* 459-495, 1995.

Sergeev, V. A., et al., Structure of the inner plasma sheet at midnight during steady convection, *Planet. Space Sci., 39,* 1083-1096, 1991.

Sergeev, V. A., et al., Event study of deep energetic particle injections during substorm, *J. Geophys. Res., 103,* 9217-9234, 1998.

Shirai, H., et al., Monoenergetic ion drop-off in the inner magnetosphere, *J. Geophys. Res., 102,* 19,873-19,881, 1997.

Smith, P. H., and R. A. Hoffman, Direct observation in the dusk hours of the characteristics of the storm time ring current particles during the beginning of magnetic storms, *J. Geophys. Res., 79,* 966-967, 1974.

Tsyganenko, N. A., Modeling the Earth's magnetospheric magnetic field confined within a realistic magnetopause, *J. Geophys. Res., 100,* 5599-5612, 1995.

Wilken, B., W. Weiss, D. Hall, M. Grande, F. Soraas, and J. F. Fennell, Magnetospheric ion composition spectrometer onboard the CRRES spacecraft, *J. Spacecr. Rockets, 29,* 585-591, 1992.

Wygant, J., et al., Experimental evidence on the role of the large spatial scale electric field in creating the ring current, *J. Geophys. Res., 103,* 29,527-29,544, 1998.

D.N. Baker and N. E. Turner, Laboratory for Atmospheric and Space Physics, University of Colorado, 1234 Innovation Drive, Boulder, CO 80303 USA. (baker@lynx.colorado.edu; niescja.turner@lasp.colorado.edu)

J. F. Fennell and J. Roeder, The Aerospace Corporation, POBox 92957, Los Angeles, CA, 90009 USA. (Joseph.F.Fennell@aero.org; James.L.Roeder@aero.org)

T. A. Fritz, Boston University, Department of Astronomy, Boston University, 725 Commonwealth Ave., Boston, MA 02215, USA. (fritz@buasta.bu.edu)

N. Yu. Ganushkina and T. I. Pulkkinen, Geophysical Research, Finnish Meteorological Institute, POBox 503, Helsinki, FIN-00101, Finland. (Nataly.Ganushkina@fmi.fi; Tuija.Pulkkinen@fmi.fi)

M. Grande and B. Kellett, Rutherford Appleton Laboratory, Chilton, Didcot, Oxfordshire, OX11, OQX, UK. (m.grande@rl.ac.uk; bjke@astro1.bnsc.rl.ac.uk)

M. V. Kubyshkina and V. A. Sergeev, University of St. Petersburg, Institute of Physics, 198904 St. Petersburg, Russia. (kubysh@snoopy.phys.spbu.ru; sergeev1@snoopy.phys.spbu.ru)

J.-A. Sauvaud, Centre d'Etude Spatial des Rayonnements, 9, Avenue du Colonel Roche, 31028 Toulouse Cedex 4, France. (Jean-Andre.Sauvaud@cesr.cnes.fr)

(Received November 18, 1999; revised April 4, 2000; accepted April 13, 2000.)